SIMULATION OF EDDY CURRENT EXAMINATION OF PRESSURE TUBES IN PHWR NUCLEAR POWER PLANTS USING DYADIC GREEN'S FUNCTIONS METHOD

Rozina Steigmann[1], Alina Bruma[2], Nicoleta Iftimie, [1], Lalita Udpa[3], Raimond Grimberg[1], Satish S. Udpa[3]

[1]National Institute of R&D for Technical Physics, Iasi, ROMANIA
[2] Al.I Cuza University, Iasi, ROMANIA
[3]Michigan State University,,East Lansing, MI, USA

Abstract
This paper presents the theoretical results obtained trough the simulation of eddy current examination of pressure tubes in PHWR nuclear power plants. The problem is purely 3D because the source that generates, the rotating field as well as the flaw are three-dimensional. To calculate the transducer's response, the dyadic Green's function method for cylindrical layered media and the method of moment's in point matching variant for flaw discretization are used.

1.INTRODUCTION

In Pressurized Heavy Water Reactor (PHWR), in pressure tubes made from Zr-2.5%Nb, the nuclear fuel bundles are inserted, and through which heavy water circulates as coolant fluid. During the functioning time, due to severe conditions of work and in the main way, due to powerful flux of thermal neutrons, the pressure tubes can present different types of flaws. During the outage, a number of pressure tubes are controlled using a combination of methods as: visual, eddy current and ultrasound. To obtain the most reliable results of the control, the using of different eddy current transducers types was proposed [1], [2], as the transducer with rotating magnetic field [3], [4]. The emphasized flaws must be distinguished of scratches made by the nuclear fuel loading –unloading machine. A diverse set of transducers has been constructed for different applications:

- Rotating transducers [5] a pancake transducer which is rotating inside the tube. Correlating the angular speed, pancake diameter and forward longitudinal speed, a full scanning of inner surface can be assured. The advantage is the allowance of the angular location of defects; also, a C-Scan of tube can be obtained. The disadvantages are due to the rotating parts that reduces the reliability and provide a slower forward speed, increasing the inspection time.
- Transducers with circumferential array of coils [6], many pancakes are disposed along the tube circumference, being connected to a multichannel eddy current equipment. If the number of coils in big enough, the precision of the angular location of defects is acceptable. The advantages are a high control speed and an angular location of the defects. The disadvantage is the increasing noise due to the vibration.
- Remote field transducers [7], used especially at the control of ferromagnetic tubes from heat exchangers.

Despite the intense research on theoretical solutions of forward and inverse problems [8, 9, 10] and experiments [11], the results in the form of a round robin test for steam generator tubes are modest. The results of the European Programme PISC III (Programme for the Inspection of Steel Components), - Action 5 on steam generator tube inspection - show that with the procedures based on eddy current testing, the inspection of axial flaws deeper than 40% of the wall thickness was often good. This capability of detection fell markedly for external flaws with a depth less than 40% of the wall thickness. In general the detection was not effective at a notification level of 20 % from the wall thickness [12], [13]. These results impose the development of new types of eddy current transducers, new operating performances, and equipment as well as signal processing and post-processing methods.

A stage in the development of new eddy current transducers is represented by the theoretical modeling of their functioning and forward problem solving. Thus, the transducer performances can be and optimized.

This paper presents the results obtained using the dyadic Green's functions methods for simulation of the response of the transducer gave at the detection of few discontinuities. For this, an absolute send-receiver transducer, using an alternative magnetic rotating field for excitation and a circumferential array of coils for reception is used.

2. THE FIELD CREATED BY AN ARBITRARY CURRENT SOURCE IN FREE SPACE, IN CYLINDRICAL COORDINATE SYSTEM

Let $\bar{J}(\bar{r})$ represent an arbitrary current source, and $e^{j\omega t}$ represent the time dependence. The field created by the source in free space is given by [14]

$$\bar{E}_0(\bar{r}) = j\omega\mu_0 \int_{Vsource} \ddot{G}_0(\bar{r},\bar{r}')\bar{J}(\bar{r}')d\bar{r}' \tag{1}$$

where $\bar{r}$ is observation point's position vector and $\bar{r}'$ is a point on source. $\ddot{G}_0$ is the dyadic Green's function for free space. This function is a dyad (3x3 matrix that transforms a vector to a vector; it is also a second rank tensor) that relates a vector field (in our case the electric field) to a vector current source.

Using a cylindrical coordinate system of $\hat{\rho},\hat{\Phi},\hat{z},$ unit vectors, the expression of $\ddot{G}_0$ for a static field source is [14]

$$\ddot{G}_0 = \ddot{I}\frac{1}{4\pi^2}\sum_{n=-\infty}^{\infty}\int_{-\infty}^{\infty} dk_z e^{j[n(\Phi-\Phi')+k_z(z-z')]} J_n(k_\rho\rho_\langle)H_n^{(1)}(k_\rho\rho_\rangle) \tag{2}$$

where $\ddot{I} = \hat{\rho}\hat{\rho} + \hat{\Phi}\hat{\Phi} + \hat{z}\hat{z}$ is unity dyad, J_n and $H_n^{(1)}$ are Bessel and Hankel first order functions, $\rho_\langle = \min(\rho,\rho'), \rho_\rangle = \max(\rho,\rho'), k_\rho = \sqrt{\omega^2\mu_0\varepsilon_0 - k_z}$ with $\mathrm{Im}(k_\rho)>0$.

In the expression of the dyad any pairs of linear independent cylindrical Bessel functions can be used, as in [14]. The source being closed

$$\begin{aligned} \nabla\bar{J} &= 0 \\ \nabla\bar{E} &= 0 \end{aligned} \tag{3}$$

the created field can be decomposed into transverse electric field (TE) in Z direction, described by f_0 potential and transverse magnetic field (TM) described by g_0 potential. In the cylindrical coordinate system, with the source having an arbitrary shape, the two components are coupled

$$\overline{E}_0(\bar{r}) = \nabla \times (\hat{z} f_0(\bar{r}) - \nabla \times \hat{z} g_0(\bar{r}))$$
$$\overline{H}_0(\bar{r}) = \frac{1}{j\omega\mu_0} \nabla \times \nabla \times (\hat{z} f_0(\bar{r}) - \nabla \times \hat{z} g_0(\bar{r})) \quad (4)$$

The source being placed in free space

$$\nabla^2 \overline{E}_0 = j\omega\mu_0 \overline{J}_0 \quad (5)$$

We calculate $\hat{z}\overline{E}_0$ as

$$\hat{z}\overline{E}_0(\bar{r}) = \hat{z}\nabla \times (\hat{z} f_0(\bar{r}) - \nabla \times \hat{z} g_0(\bar{r})) = \nabla_t^2 g_0(\bar{r}) \quad (6)$$

Where $\nabla_t = \hat{\rho}\left(\frac{1}{\rho}\frac{\partial}{\partial\rho}\right) - \hat{\Phi}\left(\frac{\partial}{\partial\rho}\right)$

Multiplying (6) by ∇^2 and taking into account (5) we obtain

$$\nabla^2 \nabla_t^2 g_0(\bar{r}) = j\omega\mu_0 \overline{J}\hat{z} \quad (7)$$

Similarly

$$\nabla^2 \nabla_t^2 f_0(\bar{r}) = j\omega\mu_0 (\nabla \times \overline{J})\hat{z} \quad (8)$$

We introduce a new function $\Gamma_0(\bar{r}, \bar{r}')$ as solution of the equation

$$\nabla_t^2 \Gamma_0(\bar{r}, \bar{r}') = G_0(\bar{r}, \bar{r}') \quad (9)$$

which has the physical significance of a potential of a singular source placed at $\bar{r}'$ so that

$$\nabla^2 \Gamma_0 = 0 \quad (10)$$

This results in

$$G_0 = -\frac{\partial^2}{\partial z^2}\Gamma_0 \quad (11)$$

so the potentials g_0 and f_0 will be

$$g_0(\bar{r}) = j\omega\mu_0 \int_{Vsource} \Gamma_0(\bar{r}, \bar{r}') \overline{J}(\bar{r}') \hat{z} d\bar{r} \quad (12)$$

$$f_0(\bar{r}) = -j\omega\mu_0 \int_{Vsource} \nabla' \times \hat{z} \Gamma_0(\bar{r}, \bar{r}') \overline{J}(\bar{r}') d\bar{r}' \quad (13)$$

Taking into account that G_0 is given by (2) , we get

$$\Gamma_0 = \frac{1}{4\pi^2} \sum_{n=-\infty}^{\infty} \int_{-\infty}^{\infty} \frac{1}{k_z^2} dk_z e^{j[n(\Phi - \Phi') + k_z(z - z')]} J_n(k_\rho \rho_\langle) H_n^{(1)}(k_\rho \rho_\rangle) \quad (14)$$

This way, the potentials g_0 and f_0 are completely determined (introducing (14) in (12) and (13)). The field created by an arbitrary source in free space, in cylindrical coordinates, is written as

$$\overline{E}_0(\bar{r}) = j\omega\mu_0 \int_{Vsource} [\nabla \times \hat{z} \bullet \nabla' \times \hat{z} \Gamma_0(\bar{r}, \bar{r}') - \nabla \times \nabla \times \hat{z} \Gamma_0(\bar{r}, \bar{r}') \bullet \hat{z}] \overline{J}(\bar{r}') d\bar{r}' \quad (15)$$

The term in the square brackets in (15) represents the free space dyad, for the case in which the current source is alternative. This has a singularity for the case $\bar{r} = \bar{r}'$ when the observation point is on the source.

For an eddy current transducer intended to the inner inspection of tubes, the field created by the current source in its exterior, case for which $\rho > \rho'$, situation in which the integral from (15) is well defined. The rotating magnetic field transducer has the components of current source written in cylindrical coordinate using the Dirac function δ the electric and magnetic fields created by the emission part are given in [15].

3. DYADIC GREEN'S FUNCTIONS FOR CYLINDRICAL LAYERED MEDIA

We consider three cylindrical layered media, delimiting the domains represented as: Ω_1 – the interior of the tube, Ω_2 – tube wall and Ω_3 – the exterior of the tube. For eddy current inspection with inner transducers, the cases presented in Figure 1 are of interest.

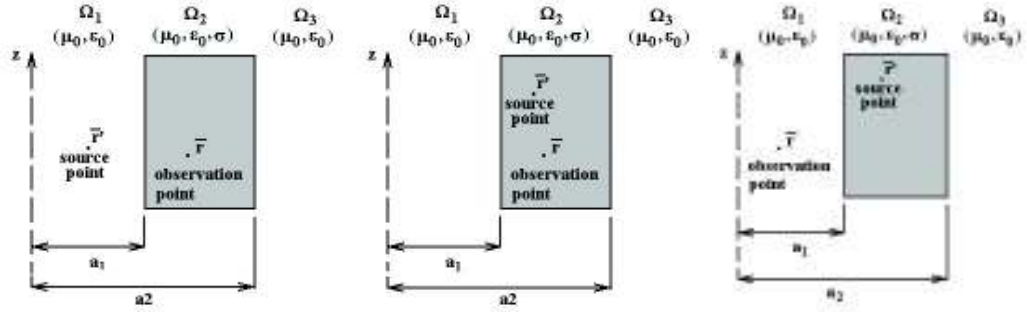

Figure 1. Relative positions of punctual current source and observation points for control of layered cylindrical media: Ω_1 - interior of tube, filled with air , Ω_2 - tube's wall, Ω_3 - exterior of tube – air; a1 – inner radius of tube; a2 – outer radius of tube: a). The source is inside the tube, observation point is in the tube's wall – for $\ddot{G}_{12}$ calculus; b) Both points are into the tube's wall – for $\ddot{G}_{22}$ calculus; c). The source is into tube's wall and observation point is inside the tube – for $\ddot{G}_{21}$ calculus

When the source is located in Ω_1 (Fig.1a), to calculate the field in Ω_2, the dyad $\ddot{G}_{12}(\bar{r},\bar{r}')$ is to be determined. The presence of a discontinuity in Ω_2, which behaves like an auxiliary current source, imposes the dyad $\overline{G}_{22}(\bar{r},\bar{r}')$ calculation (fig.1b) and to determine the emf induced in one of reception coils, the form of dyad $\ddot{G}_{21}(\bar{r},\bar{r}')$ shall be specified (fig.1c).
We note

$$k_1 = \sqrt{\omega^2\mu_0\varepsilon_0}\ ;\ k_2 = \sqrt{\omega^2\mu_0\varepsilon_0 - j\omega\mu_0\sigma}\ \ k_3 = k_1;\ k_{i\rho} = \sqrt{k_i^2 - k_z^2} \qquad \text{i =1,2,3} \tag{16}$$

3.1. $\ddot{G}_{12}$ DYAD CALCULATION

The field generated by the current source will be partially reflected at the cylindrical interface between Ω_1 and Ω_2, a part being transmitted in Ω_2 medium where it will be multiple reflected on interfaces and another part being transmitted in Ω_3 .The dyad can be calculated by two equivalent procedures:

- using the continuity conditions for the field's components on interfaces ;
- Using simple and generalized transmission and reflection coefficients [16]

Using the method presented in [16] and the geometry from Figure 1a, the dyad $\ddot{G}_{12}(\bar{r},\bar{r}')$ can be written in a matrix form as

$$\ddot{G}_{12} = \frac{j}{8\pi}\sum_{m=-\infty}^{\infty}\int_{-\infty}^{\infty} dk_z \frac{1}{\left(k_1 k_{2\rho}\right)^2}\vec{D}_\mu\left[H_n^{(1)}\left(k_{2\rho}\rho\right)\vec{I} + J_n\left(k_{2\rho}\rho\right)\overline{R}_{23}\right]$$
$$* \tilde{\tilde{M}}_2 * \tilde{\tilde{T}}_{12} * \tilde{\tilde{M}}_1 * J_n\left(k_{1\rho}\rho'\right)\vec{I}e^{j\left[n(\Phi-\Phi')+k_z(z-z')\right]}\vec{D}_\varepsilon{}^t \tag{17}$$

where

$$\begin{aligned} \bar{\bar{D}}_{\mu} &= [\nabla \times \nabla \times \hat{z}, j\omega\mu_0 \nabla \times \hat{z}] \\ \bar{\bar{\bar{D}}}' &= [\nabla' \times \nabla' \times \hat{z}, -j\omega\varepsilon_0 \nabla' \times \hat{z}] \end{aligned} \tag{18}$$

$$\begin{aligned} \tilde{\tilde{M}}_1 &= \left(\bar{\bar{I}} - \tilde{\tilde{\bar{R}}}_{12}\tilde{\tilde{\bar{R}}}_{10}\right)^{-1} = \left(\bar{\bar{I}}\right)^{-1} = I^{-1} \\ \tilde{\tilde{M}}_2 &= \left(\bar{\bar{I}} - \tilde{\tilde{\bar{R}}}_{23}\tilde{\tilde{\bar{R}}}_{21}\right)^{-1} = \left(\bar{\bar{I}} - \bar{\bar{R}}_{23}\bar{\bar{R}}_{21}\right)^{-1} \end{aligned} \tag{19}$$

$\tilde{\tilde{T}}_{12}$ is the generalized transmission coefficient from Ω_1 to Ω_2 .
The expressions for the reflection and transmission coefficients are given in Appendix A in [15].
The operator $\bar{\bar{D}}_{\mu}$ acts on the functions to its right which contains the coordinates of observation point as variables, $\bar{\bar{\bar{D}}}'^{\,t}_{\varepsilon}$ is a 2 x 3 matrix that acts on the functions to its left which contain the coordinates of current point of source as variables. The block matrix $\bar{\bar{G}}_{12}$ is of size 3X3 where each element is a (n x k_z) matrix
The field created by the source in Ω_2 will be given by

$$\bar{E}_2(\bar{r}) = j\omega\mu_0 \int_{Vsource} \bar{\bar{G}}_{12}(\bar{r}, \bar{r}')\bar{J}(\bar{r}')d\bar{r}' \tag{20}$$

For an effective field calculation, the integration order is changed so that the product between dyad and field source will be first integrated on the source volume and then the 2D inverse Fourier transform will be performed. To compute the field, the integral

$$I_1 = \int_0^{\infty} \rho' d\rho' \int_0^{2\pi} d\Phi' \int_{-\infty}^{\infty} \left[J_n\left(k_{1\rho}\rho'\right)\bar{\bar{I}}\right]\bar{J}e^{-jn\Phi' - jk_z z'}\bar{\bar{\bar{D}}}'^{\,t}_{\varepsilon} \tag{21}$$

is calculated.
Taking into account the properties of the Dirac functional, and integrating we get

$$I_1 = I_0 \begin{bmatrix} -j\frac{k_z}{k_{1\rho}} J_n\left(k_{1\rho}R\right)Rf - j\frac{n^2}{k_{1\rho}^2} f \sin\left(k_{1\rho}\frac{L_z}{2}\right)\int_0^R J_n\left(k_{1\rho}r\right)dr \\ \omega\varepsilon_0 f J_n\left(k_{1\rho}R\right) \end{bmatrix} \tag{22}$$

where f is

$$f = 1 - e^{-jn\pi} + e^{j\frac{2\pi}{3}}\left(e^{-jn\frac{2\pi}{3}} - e^{-jn\frac{5\pi}{3}}\right) + e^{j\frac{4\pi}{3}}\left(e^{-jn\frac{\pi}{3}} - e^{-jn\frac{4\pi}{3}}\right) \tag{23}$$

The function f is periodic, with period 6, having nulls for even n.
Because the source and the observation points are in different media, the dyad doest not encounter any singularities, and the integrals are hence well defined.

3.2. $\bar{\bar{G}}_{22}$ DYAD CALCULATION

In the geometry presented in Figure 1b, the source and the observation points are in the same medium. In principle, the form of $\bar{\bar{G}}_{22}$ dyad will be similar to $\bar{\bar{G}}_0$ and the terms that characterize the reflection on cylindrical interfaces must be included. Using the method presented in [16], two different expressions of the dyad will be obtained, one for $\boldsymbol{\rho} > \boldsymbol{\rho}'$ and the other for $\boldsymbol{\rho} < \boldsymbol{\rho}'$. If $\rho = \rho'$, the dyad presents a singularity that should be treated separately. Therefore, it can be written as

$$\ddot{G}_{22}(\bar{r},\bar{r}') = \frac{j}{8\pi^2}\sum_{n=-\infty}^{\infty}\int_{-\infty}^{\infty} dk_z \frac{1}{\left(k_2 k_{2\rho}\right)^2}\overline{D}_\mu \overline{F}_n\left(\rho,\rho'\right)e^{jn(\Phi-\Phi')+k_z(z-z')}\overline{\overline{D}}_\varepsilon + \frac{\hat{\rho}\hat{\rho}}{k_2^{\,2}}\delta(\bar{r}-\bar{r}') \quad (24)$$

where

$$\overline{F}_n\left(\rho,\rho'\right) = \begin{cases} \left[H_n^{(1)}\left(k_{2\rho}\rho\right)\overline{I} + J_n\left(k_{2\rho}\rho\right)\tilde{\tilde{R}}_{23}\right] * \tilde{\tilde{M}}_2 \\ *\left[J_n\left(k_{2\rho}\rho'\right)\overline{I} + H_n^{(1)}\left(k_{2\rho}\rho'\right)\tilde{\tilde{R}}_{21}\right] \end{cases} for \quad \rho > \rho' \\ \begin{cases} \left[J_n\left(k_{2\rho}\rho\right)\overline{I} + H_n^{(1)}\left(k_{2\rho}\rho\right)\tilde{\tilde{R}}_{21}\right] * \tilde{\tilde{M}}_2 \\ *\left[H_n^{(1)}\left(k_{2\rho}\rho'\right)\overline{I} + J_n\left(k_{2\rho}\rho'\right)\tilde{\tilde{R}}_{23}\right] \end{cases} for \quad \rho < \rho' \quad (25)$$

To calculate the field, the dyad must be multiplied with the current source, integrated on source volume and then the 2D inverse Fourier transform must be preformed.

3.3 $\ddot{G}_{21}$ DYAD CALCULATION

This situation is presented in Figure 1c, where the source is in Ω_2 and the observation point is in Ω_1. Consequently there are no singularities and the integrals are defined.

$$\ddot{G}_{21}(\bar{r},\bar{r}') = \frac{j}{8\pi^2}\sum_{n=-\infty}^{\infty}\int_{-\infty}^{\infty}\frac{1}{\left(k_2 k_{2\rho}\right)^2}\overline{D}_\mu\left[J_n\left(k_{1\rho}\rho\right)\overline{I}\right] * \tilde{\tilde{M}}_1 * \tilde{\tilde{T}}_{21} * \tilde{\tilde{M}}_2$$
$$\left[H_n^{(1)}\left(k_{2\rho}\rho'\right)\overline{I} + J_n\left(k_{2\rho}\rho'\right)\tilde{\tilde{R}}_{23}\right]e^{jn(\Phi-\Phi')+jk_z(z-z')}\overline{\overline{D}}_\varepsilon \quad (27)$$

4. FORWARD PROBLEM FOR ROTATING MAGNETIC FIELD TRANSDUCER

For the detection of material discontinuities the emission part of the rotating magnetic field transducer is connected to a reception part consisting of an arbitrary number of coils, placed in a circumferential array, as shown in Figure 2.

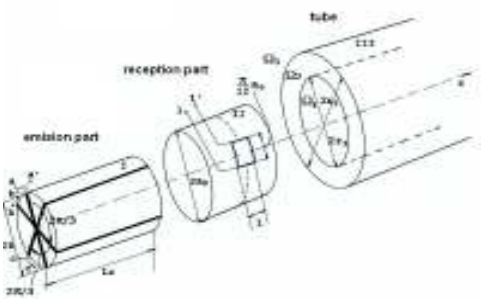

Figure 2. Principle scheme of inner eddy current transducer with rotating magnetic field

The emf. induced in the reception coils will be modified, as result of the field associated with the inhomogeneities in the tube walls material. With a large number of reception coils a higher circumferential resolution can be achieved.

The forward problem was solved using the dyadic Green's functions for cylindrical layered media, presented in [15], and the integral on source volume.

The flaws existing in the tube wall will behave as auxiliary current sources with density

$$\overline{J}_f(\bar{r}) = [\sigma_0(\bar{r}) - \sigma]\overline{E}_d(\bar{r}) \quad (28)$$

where $\sigma_0(\bar{r})$ is the conductivity of medium that fills the flaw, and $\bar{E}_d(\bar{r})$ is the scattered field. The electric fields in the tube wall are related according to

$$\bar{E}_2(\bar{r}) = \bar{E}_d(\bar{r}) - j\omega\mu_0\sigma \int_{Vflaw} \ddot{G}_{22}(\bar{r},\bar{r}')\frac{1}{\sigma}\bar{J}_f(\bar{r}')d\bar{r}' \tag{29}$$

where $\bar{E}_2(\bar{r})$ is the incident field induced in the tube wall in the absence of any flaws, by the emission part.

Equation (29) was discretized using the moment method [17], the flaw zone being divided into $N_\rho \times N_\Phi \times N_z$ cells with $\Delta\rho \times \Delta\Phi \times \Delta z$ dimensions small enough so that the incident field and the scattered field are considered constant within the cell's volume and equal to the value in the centre of the cell. The centres of cells are indicated by (k,l,m) with k=1,2,…N_ρ, l=1,2,…N_Φ , m=1,2,…N_z .

Using point-matching variant of moment's method [18] and taking into account the equation (28), the Freedholm integral equation (29) is transformed into a algebraic system of equations

$$E_2(\rho_K,\Phi_L,z_M) = E_d(\rho_K,\Phi_L,z_M) - j\omega\mu_0\sigma\sum_{k=1}^{N_\rho}\sum_{l=1}^{N_\Phi}\sum_{m=1}^{N_z}U(\rho_K,\Phi_L,z_M,\rho_k,\Phi_l,z_m) \tag{30}$$
$$* \chi(\rho_k,\Phi_l,z_m)E_d(\rho_k,\Phi_l,z_m)$$

where

$$\chi(\rho_k,\Phi_l,z_m) = \frac{\sigma_0(\rho_k,\Phi_l,z_m)-\sigma}{\sigma} \tag{31}$$

$$U(\rho_K,\Phi_L,z_M,\rho_k,\Phi_l,z_m) = \int_{\Delta\rho}\rho'd\rho' \int_{\Delta\Phi} d\Phi' \int_{\Delta z} dz' G_{22}(\rho_K,\Phi_L,z_M,\rho',\Phi',z') \tag{32}$$

G_{22} is given by (25) and (26).

The calculation of U was performed as follows:

a) The integration on Φ' and z' was performed; these variables appear only in complex exponentials.

$$\int_{\Phi_l-\frac{\Delta\Phi}{2}}^{\Phi_l+\frac{\Delta\Phi}{2}} e^{-jn\Phi'}d\Phi' = \Delta\Phi\sin c\left(n\frac{\Delta\Phi}{2}\right)e^{-jn\Phi_l}$$

$$\int_{z_m-\frac{\Delta z}{2}}^{z_m+\frac{\Delta z}{2}} e^{-jk_z z'}dz' = \Delta z\sin c\left(k_z\frac{\Delta z}{2}\right)e^{-jk_z z_m}$$

b) The integration on ρ' was performed as described below: we note with $I_2(\rho')$ the integrand in (25) for ρ<ρ' and with $I_3(\rho')$ the integrand in (26) for ρ>ρ'.

The integral after ρ' from (32) can be written as

$$\int_{\rho_k-\frac{\Delta\rho}{2}}^{\rho_k-\varepsilon} I_2(\rho')\rho'd\rho' + \int_{\rho_k+\varepsilon}^{\rho_k+\frac{\Delta\rho}{2}} I_3(\rho')\rho'd\rho' \tag{33}$$

In this way, the singularity from ρ_k is avoided. The integrals from (33) cannot be analytically calculated. It was chosen $\varepsilon = 10^{-5}\rho_k$ and then each integral were numerically calculates using the 3[rd] order Gauss quadrature,

c) to ρ, Φ, z, the values corresponding to flaw's discretization cells centers coordinates are assigned, thus ρ_K, Φ_L, z_M.

E_2, the electric field in the flawless material without flaw, is given by (20). The equations system (30) is solved in Fourier space. To determine E_d, the field scattered in the material, the inverse generalized matrix method, in Moore-Penrose sense, was used.

To simulate the transducer displacement into the controlled tube, the supplementary factor $e^{jk_z z_b}$ was introduced, where z_b is a vector that contains the successive positions of the transducer. For each transducer position, the field in flaw's discretization cells centres is calculated and the system (30) is solved, $E_{d\rho}(\rho,\Phi,z)$, $E_{d\Phi}(\rho,\Phi,z)$ and $E_{dz}(\rho,\Phi,z)$ - the scattered field components values - being obtained.

The knowledge of scattered field in material, [in other words, the field created by auxiliary current source (the discontinuity)], immediately allows the determination of their current density and, using the dyadic Green's function $\ddot{G}_{21}(\bar{r},\bar{r}')$, the field scattered in air can be calculated.

$$\bar{E}_2(\rho,\Phi,z) = \int_{Vflaw} \ddot{G}_{21}(\bar{r},\bar{r}')\bar{J}_f(\bar{r}')d\bar{r}' \tag{34}$$

where $\ddot{G}_{21}(\bar{r},\bar{r}')$ is given by (27), and $\bar{J}_f(\bar{r})$ is given by (28) with $\bar{E}_d(\bar{r})$ solution of (30).

The electromotive force induced in one of reception coils, presented in Figure 2, will be

$$e = \oint_{\Psi} \bar{E}_2 d\bar{l} \tag{35}$$

where Ψ represents the reception coil's outline. If the reception coils are disposed on a circumference, with R_1 radius, the curvilinear integral from (35) can be written

$$e = \int_{z_1}^{z_2} E_{2_z}(R_1,\Phi_1,z)dz + \int_{\Phi_1}^{\Phi_2} E_{2_\Phi}(R_1,\Phi,z_2)d\Phi + \int_{z_2}^{z_1} E_{2_z}(R_1,\Phi_2,z)dz + \int_{\Phi_2}^{\Phi_1} E_{2_\Phi}(R_1,\Phi,z_1)d\Phi \tag{36}$$

From (36) results that for the calculation of the induced emf, only 2 components of the field scattered by the flaw in air, are needed. Due to the integrals which are made in report with Φ and z, variables that appear only at exponent, the calculus is analytic, directly.

In final, 2D inverse Fourier transforms are performed, using trapezium method. Therefore, to solve the forward problem, the calculi are made in Fourier space, and only in final, the inverse Fourier transform is made. For a discontinuity from the wall's tube discretized into 10 cells, the elements number of one dyad $\ddot{G}_{22}$ component (from 9 components) will be 129x129x10x10=1.664.100 elements, using approximate 52Mb RAM.

5. NUMERICAL SIMULATION

A Matlab 7 numerical code was developed to predict the response of the transducer. The simulated situations were for a tube with inner radius 52.5 mm, outer radius 56.66 mm, made from Zr2.5%Nb alloy, having $1.89*10^6$ S/m electrical conductivity.

On tube, three discontinuities were considered, being presented in Table 1.

Table 1. The discontinuities features

No.	Location	Type	Dimensions [mm]			Discretization [cells]
			Axial	Circumferential	Depth	
7	OD	Rubbing mark	16	8	0.2	16 x 8 x 1
8	ID	Circumferential	0.2	11	0.2	1 x 11 x 1
9	OD	Axial	6	0.2	1	6 x 1 x 5

The characteristics of the transducer that has been used are R=50mm; Lz=60mm; each of the 3 rectangular emission coils has 70 turns, the amplitude of tri-phased current is 0.1A, frequency 40kHz. For reception, each coil has 8.0mm axial dimension and 10.0mm circumferential dimension, 70 turns, disposed on a cylindrical surface with 52.0mm radius. In each situation the transducer was considered as being centred above the discontinuity. The scanning step and the start position were choosen so that the simulation results shall present the expected symmetry. The results obtained by simulations are presented in Figures 3 a, b and c.

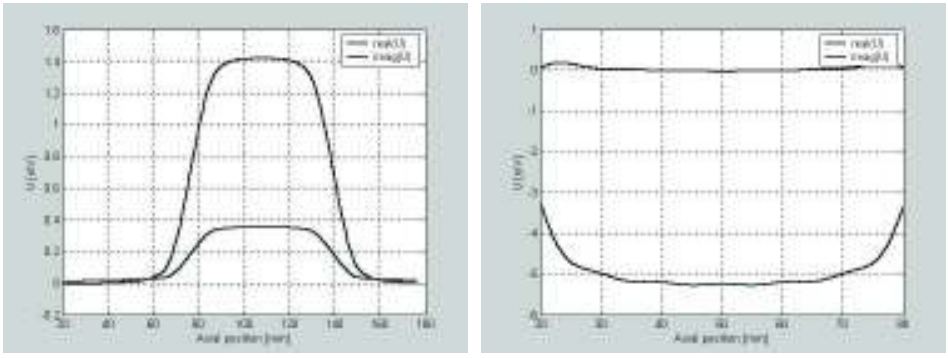

a b

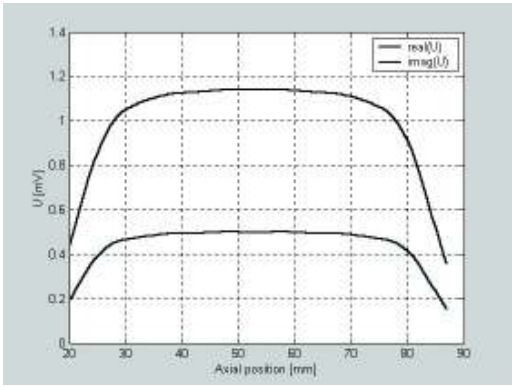

c

Figure 3. Simulation results
a – for #7 – OD rubbing mark (axial dimension 16mm, circumferential 8mm, depth 0.2mm);
b – for #8 – ID circumferential (axial dimension 0.2mm, circumferential 11mm, depth 0.2mm);
c – for #9 – OD axial (axial dimension 6mm, circumferential 0.4mm, depth 1mm)

To verify these results, an eddy current inner transducer with rotating magnetic field and adequate equipments were realized [19]. The tube, the discontinuities, the transducer and the experimental conditions are the same as for the simulations.
Comparing the simulation results (figs. 3a, b and c) with experimental ones [19], a good correlation can be observed. The experimental data contains noises due to the variable lift-off at transducer displacing into the tube. The diameter of the transducer shall be smaller than the inner diameter of tube to assure the displacement without friction.

6. CONCLUSIONS

For the transducer with rotating magnetic field, the forward problem was solved using the volume integral method and the dyad Green's functions for layered cylindrical media. The

prediction of transducer response was made for three discontinuities placed in both the inner and the outer surface of the tube sample made from Zr2.5%Nb alloy. For these discontinuities, experimental measurements were made, being in good concordance with the solutions of the forward problem.

REFERENCES

1. V.S. Cecco, G. Van Drunnen, F.L. Sharp, "Manual on eddy current method", Vol.1, Chalk River Nuclear Laboratories, revision 1 (1983)
2. Nondestructive Testing Handbook, vol.5, Electromagnetic Testing: S.S.Udpa, P.O.Moore Eds, ASNT, 2004
3. A. Savin, L. Udpa, R. Steigmann, R. Grimberg and S. Udpa,, Nondestructive examination of fuel channels in PHWR nuclear power plants, *International Journal of Materials and Product Technology,vol.27, nos.3/4, 2006, pp.198-209*
4. R. Grimberg, Lalita Udpa, Adriana Savin, Rozina Steigmann, Satish S. Udpa, Inner Eddy Current Transducer with Rotating Magnetic Field; Experimental Results: Application to NDE of Pressure Tubes, in PHWR Nuclear Power Plants, Research in Nondestructive Evaluation, 2005, Springer-Verlag New York, LLC, vol 16, issue 2, pp. 65-78
5. R.C.McMaster, Nondestructive Testing Handbook, Second edition, ASNT, London , 1986
6. G.Lafontaine,F.Hardy,J.Renaud – X probe ECT array; a high-speed Replacement for Rotating Probes, NDT.net, 7,8,(2002), ISSN: 1435-4934
7. Y. Sun, J. T. Si, D. Cooley, H. C. Han, S. S. Udpa, W. Lord, M. Qu, M. Chen, and Y. Zhao, "Efforts Towards Gaining a Better Understanding of the Remote Field Eddy Current Phenomenon and Expanding its Applications," IEEE Transactions on Magnetics, Vol. 32, No. 3, pp. 1589-1592, 1996.
8. H.A.Sabbagh, L.D. Sabbagh, Development of a system to invert eddy current data and reconstruct flaws, International Advances in Nondestructive Testing, 1984, vol.10, p.267-305
9. H.A.Sabbagh, L.D. Sabbagh, Inversion of eddy current data and the reconstruction of flaws using multifrequencies, International Advances in Nondestructive Testing, 1984, vol.10, p.307-332
10. C.Lemenager, R.Zorgati, C.Cloarec, P.Jardet, H.Jacquot, 2D Eddy current Imaging for Steam Generator Tubing, in Electomagnetic Nondestructive Evaluation(II), eds. R.Albanese, G.Rubinacci, T.Takagi, S.S.Udpa, IOS Press, Amsterdam,1998, pp251-260
11. K.Miya, Progress of Tube inspection Technology in Nuclear Power Plant of Japan, in Nondestructive Testing of Materials, R.Collins &all(eds), IOS Press, Amsterdam,1995, pp.341-347
12. M.Bieth, C.Birac, R.Comby, G.Magica, W.Neumann, Final Results of the PISC III Round Robin Test on Steam Generator Tube Inspection, First International Conference on NDE in Relation to Structural Integrity for Nuclear and Pressurized Components, 20 - 22 October 1998, Amsterdam, Netherlands
13. M.Bieth, C.Birac, R.Comby, G.Magica, W.Neumann, Final Results of the PISC III Round Robin Test on Steam Generator Tube Inspection, The e-Journal of Nondestructive Testing, NDT.net,vol.4,no.10,(1999)
14. J.D. Jackson, Classical Electrodynamics, 3[rd] Edition, John Wiley &Sons, NY, 1999
15. R. Grimberg, Lalita Udpa, Adriana Savin, Rozina Steigmann, S. Udpa, INNER EDDY CURRENT TRANSDUCER WITH ROTATING MAGNETIC FIELD. THEORETICAL MODEL – FORWARD PROBLEM, Research in Nondestructive Evaluation, 2005, Springer-Verlag New York, LLC, vol 16, issue 2,pp.79-100
16. W.Cho Chew, Waves and Fields in inhomogeneous media, Van Nostrand Reinhold, NY, chapter 3 and 7.
17. R.F.Harrington, Field Computation by moment method, ed.II, Wiley-IEEE Pres,.N.Y.,1993
18. R.H.T.Bates, IEEE trans. Microwave Theory Tech,15,(1967),pp185-198
19. R. Grimberg, Lalita Udpa, Adriana Savin, Rozina Steigmann, Satish S. Udpa, INNER EDDY CURRENT TRANSDUCER WITH ROTATING MAGNETIC FIELD; EXPERIMENTAL RESULTS: APPLICATION TO NONDESTRUCTIVE EXAMINATION OF PRESSURE TUBES IN PHWR NUCLEAR POWER PLANTS, Research in Nondestructive Evaluation, 2005, Springer-Verlag New York, LLC, vol 16, issue 2, pp. 65-78

ACKNOWLEDGMENTS

This paper is partially supported by Romanian Ministry of Education and Research under Excellence Research Program – Contract no. 6110/2005 CEEX CALIST- Project SINERMAT, and Nucleus Program, Contract no.06-38-01.03